Anal. Chem. **2008,** *80,* 5839–5846

In Vivo Detection of Superoxide Anion in Bean Sprout Based on ZnO Nanodisks with Facilitated Activity for Direct Electron Transfer of Superoxide Dismutase

Zifeng Deng, Qi Rui, Xia Yin, Haiqing Liu, and Yang Tian*

Department of Chemistry, Tongji University, Siping Road 1239, Shanghai 200092, P. R. China

Here, we report on a novel superoxide anion ($O_2^{\bullet-}$) biosensor based on direct electron transfer of copper, zinc-superoxide dismutase (Cu, Zn-SOD) at zinc oxide nanodisks surface for in vivo tracking of $O_2^{\bullet-}$ in bean sprouts. Direct electron transfer of SOD is achieved at ZnO nanodisks film prepared by a one-step electrodeposited method, with a high heterogeneous electron rate constant of $17 \pm 2\ s^{-1}$. Spectroscopic data demonstrate that SOD strongly immobilized onto the nanostructured ZnO surfaces processes its inherent activity toward $O_2^{\bullet-}$ dismutation. A combination of the facilitated direct electron transfer and the bifunctional enzymatic catalytic activities of the SOD substantially provides a dual electrochemical approach to determination of $O_2^{\bullet-}$ with high selectivity, wide linear range, long stability, and good reproducibility. In particular, SOD adsorbed on the ZnO nanodisks film is capable of sensing $O_2^{\bullet-}$ cathodically at a very positive potential, 0 mV (vs Ag|AgCl), where the common interfering species such as hydrogen peroxide, uric acid, ascorbic acid, and 3,4-dihydroxyphenylacetic acid were effectively avoided. The excellent analytical performance of the present $O_2^{\bullet-}$ biosensor, combined with the remarkable characteristics of nanostructured ZnO films, such as biocompatibility, ease of preparation, and facile to miniaturize, paves an electrochemical way for reliable and durable in vivo determination of $O_2^{\bullet-}$ in bean sprouts.

Superoxide anion ($O_2^{\bullet-}$), the primary species of the reactive oxygen species (ROS), plays a central role in physiological processes.[1–3] Under normal metabolic conditions, $O_2^{\bullet-}$ is produced at a rate that is matched by the capacity of tissue to catabolize them.[4] When its production exceeds the body's natural ability to deal with the potentially cytotoxic species, a variety of pathological conditions may result including cancer, stroke, and neurodegeneration.[5] In plants, $O_2^{\bullet-}$ is commonly produced in illuminated chloroplasts by the occasional transfer of an electron from an excited Chl molecule or PSI components under conditions of high NADPH/NADP ratios to molecular O_2.[6] Various environmental perturbations, such as hyperoxia, herbicides, pathogens, ozone, temperature fluctuations, and other stresses are known to induce $O_2^{\bullet-}$ formation in most aerobic organisms.[6]

In order to gain a full understanding of the role that $O_2^{\bullet-}$ and ROS plays in pathology and physiology and the relationship between $O_2^{\bullet-}$ and environmental stresses, it is essential to determine $O_2^{\bullet-}$ in a variety of in vitro and in vivo models. However, it is still an analytical challenge to detect the local concentration of $O_2^{\bullet-}$, especially in the biological systems, because of its low concentration, high reactivity, and short lifetime. Over the past years, considerable attention has been paid to the detection of $O_2^{\bullet-}$, and a lot of techniques, such as spectrometry, fluorometry, chemiluminensence, and electron spin resonance, have been developed.[7–11] Recent attempts have concentrated on electrochemical methods due to their direct, real-time measurements and capability for in vivo detection. Mostly, copper, zinc-superoxide dismutase (Cu, Zn-SOD)-immobilized electrodes have paved an elegant way to detect $O_2^{\bullet-}$. SODs catalyze the dismutation of $O_2^{\bullet-}$ to O_2 and H_2O_2 via a cyclic oxidation−reduction electron-transfer mechanism and are widely distributed among aerobic organisms. SODs show high rate constants, up to the order of $10^9\ M^{-1}\ S^{1-}$, and are distinguished by a highly uncommon specificity to $O_2^{\bullet-}$.[12–14] Therefore, SOD, a specific enzyme for $O_2^{\bullet-}$ dismutation, offers great potential for the sensitive and selective quantification of $O_2^{\bullet-}$ in electrochemical biosensors. The SOD-based first-generation biosensors have been constructed on the detection of H_2O_2 produced from $O_2^{\bullet-}$ dismutation catalyzed by SOD. However,

* To whom correspondence should be addressed. E-mail: yangtian@mail.tongji.edu.cn. Tel: +86-21-65987075. Fax: +86-21-65982287.

(1) Auchere, F.; Rusnak, F. *J. Biol. Inorg. Chem.* **2002**, *7*, 664–667.
(2) Dean, R. T.; Fu, S.; Stocker, R.; Davies, M. J. *Biochem. J.* **1997**, *324*, 1–18.
(3) Halliwell, B.; Gutteridge, J. M. C. *Biochem. J.* **1984**, *219*, 1–14.
(4) Van Lente, F. *Anal. Chem.* **1993**, *65*, 374R–377R
(5) Halliwell, B.; Gutteridge, J. M. C. *Arch. Biochem. Biophys.* **1986**, *246*, 501–514.
(6) Scandalios, J. G. *Plant Physiol.* **1993**, *101*, 7–12.
(7) Zweier, J. L.; Flaherty, J. H.; Weisfeldt, M. L. *Proc. Natl. Acad. Sci. U. S. A.* **1987**, *84*, 1404–1047.
(8) Ohara, Y.; Peterson, T. E.; Harrison, D. G. *J. Clin. Invest.* **1993**, *91*, 2546–2551.
(9) Vasquez-Vivar, J.; Hogg, N.; Pritchard, K. A.; Kalyanaraman, B. *FEBS Lett.* **1997**, *403*, 127–130.
(10) Zhang, H.; Joseph, J.; Vasquez-Vivar, J.; Karoui, H.; Nsanzumuhire, C.; Martasek, P.; Tordo, P.; Kalyanaraman, B. *FEBS Lett.* **2000**, *473*, 58–62.
(11) Ohyashiki, T.; Nunomura, M.; Katoh, T. *Biochim. Biophys. Acta* **1999**, *1421*, 131–139.
(12) McCord, J. M.; Fridovich, I. *J. Biol. Chem.* **1969**, *244*, 6094–6055.
(13) Fridovich, I. In *Superoxide Dismutase*; Oberley, L. W., Ed.; CRC Press: Boca Raton, FL, 1982; Vol. 1, Chapter 3.
(14) *Superoxide Dismutase*; Oberley, L. W., Ed.; CRC Press: Boca Raton, FL, 1985; Vol. 3.

10.1021/ac800213x CCC: $40.75
Published on Web 07/02/2008

the high potential required for the oxidation of H_2O_2 may cause the simultaneous oxidation of some coexisting electroactive species in biological samples. Meanwhile, the biosensors based on the detection of H_2O_2 seem to be limited in differentiation of H_2O_2 produced by the SOD-catalyzed dismutation of $O_2^{\bullet-}$ from that endogenously produced in the biological systems.[15–18] The second-generation $O_2^{\bullet-}$ biosensor is based on the electron transfer of SOD realized by surface-confined mediators (or solution-phase Me_{ox}/M_{red} couple).[19] To construct the selective and sensitive third-generation biosensors for $O_2^{\bullet-}$, much effort has been paid to direct electron transfer of SODs.

A reversible redox response of bovine and human Cu, Zn-SOD was first observed on a gold electrode in the presence of the so-called electron-transfer promoters.[20–24] The electrochemistry of SODs has been systematically studied and the direct electron transfer of not only Cu, Zn-SOD but also Fe-SOD and Mn-SOD has been successfully realized with the self-assembled monolayer confined on a gold electrode. On the basis of these results, sensitive and selective SOD-based third-generation $O_2^{\bullet-}$ biosensors have been developed with good linearity in the nanomolar range and a low detection limit.[25–31] However, from the view of in vivo applications, the above-mentioned $O_2^{\bullet-}$ biosensors are still up against the following requirements: the implantable miniature of electrodes; stability and reproducibility of biosensors; and most importantly, wide dynamic linear range, not only in nanomolar concentration but also up to micromolar and even millimolar grade concentration of $O_2^{\bullet-}$. It is well-known that, under normal physiological conditions, $O_2^{\bullet-}$ undergoes disproportionation by non-catalytic and enzymatic reactions, resulting in a rather low physiological concentration (10^{-8}–10^{-7} M). Increases in the activity of $O_2^{\bullet-}$ occur in response to traumatic brain injury ischemia−reperfusion, hypoxia, and environmental stresses; the concentration of $O_2^{\bullet-}$ may increase to $\sim 10^{-4}$ M. So, it is essential to provide quantitative information on $O_2^{\bullet-}$ concentration ranging from the nanomolar level to millimolar grade for tracking the role that $O_2^{\bullet-}$ plays in physiological and pathological processes.

In order to challenge these key analytical problems for in vivo determination of $O_2^{\bullet-}$, in the present work, it is the first time that direct electron transfer of Cu, Zn-SOD was achieved at electrodeposited nanostructured ZnO disks without any mediators or promoters. Nanostructured metal oxide films, such as TiO_2 and ZnO, have found extensive applications in solar cells, environmental purification, electronic devices, gas sensors, and so on due to their remarkable chemical, electronic, and optical characteristics.[32–34] Recently, TiO_2 nanoparticles and nanotubes were reported useful for the immobilization of heme proteins and biomaterials for the development of optical and electrochemical biosensors and for studying interactions between proteins and electrodes.[35–42] Unfortunately, to the best of our knowledge, few reports were concerned with the direct electron transfer of proteins or enzymes at ZnO films,[42,43] in spite of its notable properties, e.g., high surface area, optical transparency, nontoxicity, ease of preparation, chemical and photochemical stability, and electrochemical activity. Moreover, compared to TiO_2, ZnO exhibits two remarkable characteristics: one is a higher isoelectric point, implying that ZnO may have more benefit for the adsorption of proteins with low isoelectric points than TiO_2. Another is that ZnO demonstrates a slightly lower conduction band edge and higher density of sub-band gap states than TiO_2, resulting in significant conductivities and electrochemical activities.[42,44,45]

Here, as expected, direct redox reaction of Cu, Zn-SOD with a low isoelectric point ($pI = 4.9$) was realized at the ZnO nanodisks film. The experimental data revealed that the nanostructured ZnO film stably immobilized SOD molecules and SOD processed its intrinsic activity toward dismutation for $O_2^{\bullet-}$. The ZnO-SOD nanocomposites showed a bifunctional electrocatalytic activity toward $O_2^{\bullet-}$, in which $O_2^{\bullet-}$ could be detected both anodically and cathodically. Besides high selectivity, the present third-generation $O_2^{\bullet-}$ biosensor exhibited excellent analytical performance, such as wide dynamic linear range, long stability, and good reproducibility. These characteristics, together with the remarkable properties of nanostructured ZnO film, sufficiently offered an electrochemical approach to in vivo detection of $O_2^{\bullet-}$ in bean sprouts.

(15) Mesaros, S.; Vankova, Z.; Grunfeld, S.; Mesarosova, A.; Malinski, T. *Anal. Chim. Acta* **1998**, *358*, 27–30.
(16) Song, M. I.; Bier, F. F.; Scheller, F. W. *Bioelectrochem. Bioenerg.* **1995**, *38*, 419–422.
(17) McNeil, C. J.; Greenough, K. R.; Weeks, P. A.; Self, C. H. *Free Radical Res. Commun.* **1992**, *17*, 399–406.
(18) Lvovich, V.; Scheeline, A. *Anal. Chem.* **1997**, *69*, 454–462.
(19) Endo, K.; Miyasaka, T.; Mochizuki, S.; Himi, N.; Asahara, H.; Tsujioka, K.; Sakai, K. *Sens. Actuators, B* **2002**, *83*, 30–34.
(20) Borsari, M.; Azab, H. A. *Bioelectrochem. Bioenerg.* **1992**, *27*, 229–233.
(21) Azab, H. A.; Banci, L.; Borsari, M.; Luchinat, C.; Sola, M.; Viezzoli, M. S. *Inorg. Chem.* **1992**, *31*, 4649–4655.
(22) Wu, X.; Meng, X.; Wang, Z.; Zhang, Z. *Chem. Lett.* **1999**, *12*, 1271–1272.
(23) Wu, X.; Meng, X.; Wang, Z.; Zhang, Z. *Bioelectrochem. Bioenerg.* **1999**, *48*, 227–231.
(24) Ge, B.; Scheller, F. W.; Lisdat, F. *Biosens. Bioelectron.* **2003**, *18*, 295–302.
(25) Tian, Y.; Shioda, M.; Kasahara, S.; Okajima, T.; Mao, L.; Hisaboli, T.; Ohsaka, T. *Biochim. Biophys. Acta* **2002**, *1569*, 151–158.
(26) Tian, Y.; Mao, L.; Okajima, T.; Ohsaka, T. *Anal. Chem.* **2002**, *74*, 2428–2434.
(27) Ohsaka, T.; Tian, Y.; Shioda, M.; Kasahara, S.; Okajima, T. *Chem. Commun.* **2002**, 990–991.
(28) Tian, Y.; Mao, L.; Okajima, T.; Ohsaka, T. *Anal. Chem.* **2004**, *76*, 4162–4168.
(29) Tian, Y.; Ariga, T.; Takashima, N.; Okajima, T.; Mao, L.; Ohsaka, T. *Electrochem. Commun.* **2004**, *6*, 609–614.
(30) Tian, Y.; Mao, L.; Okajima, T.; Ohsaka, T. *Biosens. Bioelectron.* **2005**, *21*, 557–564.
(31) Tian, Y.; Mao, L.; Ohsaka, T. *Current Anal. Chem.* **2006**, *2*, 51–58.
(32) O'Regan, B.; Gratzel, M. *Nature* **1991**, *353*, 737–739.
(33) Baughman, R. H.; Zakhidov, A. V.; De Heer, W. A. *Science* **2002**, *297*, 787–793.
(34) Senda, S.; Sakai, Y.; Mizuta, Y.; Kita, S.; Okuyama, F. *Appl. Phys. Lett.* **2004**, *85*, 5679–5681.
(35) Saito, Y.; Uemura, S. *Carbon* **2000**, *38*, 169–182.
(36) Huang, M.; Mao, S.; Feick, H.; Yan, H.; Wu, Y.; Kind, H.; Weber, E.; Russo, R.; Yang, P. *Science* **2001**, *292*, 1897–1899.
(37) Fancher, C. A.; De Clercq, H. L.; Thomas, O. C.; Robinson, D. W.; Bowen, K. H. *J. Chem. Phys.* **1998**, *109*, 8426–8429.
(38) Liu, A.; Wei, M.; Honma, I.; Zhou, H. *Anal. Chem.* **2005**, *77*, 8068–8077.
(39) Topoglidis, E.; Lutz, T.; Willis, R. L.; Barnett, C. J.; Cass, A. E. G.; Durrant, J. R. *Faraday Discuss.* **2000**, *116*, 35–46.
(40) Topoglidis, E.; Campbell, C. J.; Cass, A. E. G.; Durrant, J. R. *Langmuir* **2001**, *17*, 7899–7906.
(41) Topoglidis, E.; Astuti, Y.; Duriaux, F.; Gratzel, M.; Durrant, J. R. *Langmuir* **2003**, *19*, 6894–6900.
(42) Topoglidis, E.; Cass, A. E. G.; O'Regan, B.; Durrant, J. R. *J. Electroanal. Chem.* **2001**, *517*, 20–27.
(43) Zhang, C.; Liu, M.; Li, P.; Xian, Y.; Cheng, Y.; Zhang, F.; Wang, X.; Jin, L. *Chin. J. Chem.* **2005**, *23*, 144–148.
(44) Kar, S.; Pal., B. N.; Chaudhuri, S.; Chakravorty, D. J. *Phys. Chem. B* **2006**, *110*, 4605–4611.
(45) Bae, S. Y.; Seo, H. W.; Park, J. *J. Phys. Chem. B* **2004**, *108*, 5206–5210.

EXPERIMENTAL SECTION

Chemicals and Materials. Bovine erythrocyte Cu, Zn-SOD (MW 32 000) was obtained from Sigma and used without further purification. Phosphate buffer solution (PBS, 25 mM) was prepared by mixed stock standard K_2HPO_4 and KH_2PO_4 solutions, and pH of PBS was adjusted by pH meter. Other reagents were of analytical grade and used as received. ITO-coated glass plates with a square resistance of 10−20 Ω cm^{-2} were obtained from Asahi Glass. A stock solution of KO_2 was prepared by adding KO_2 to DMSO (stored together with molecular sieve 4Å (Wako Pure Chemical Industries, Ltd.)), sonicating the solution for 5min. All the solutions were prepared with Milli-Q water and were deaerated with high-purity nitrogen before experiments.

Preparation and Modification of Nanostructured ZnO Film. ITO-coated glass plates were thoroughly cleaned by sonication for 30 min in the following solvents successively: soapy water, neat ethanol, 1 M NaOH, and water. A ZnO nanodisks film was electrodeposited on an ITO glass plate from 0.1 mM $Zn(NO_3)_2$ solution containing 0.1 mM KCl at the applied potential of −0.9 V versus Ag|AgCl for 20 min. and then sintered at 773 K for 0.5−1.5 h. The nanostructured ZnO film was modified with Cu, Zn-SOD by immersing the ZnO film into PBS (pH 7.2) of Cu, Zn-SOD (0.2 mM) for ∼0.5−3 h at 3 °C in a refrigerator. Hereafter, Cu, Zn-SOD modified-nanostructured ZnO electrode will be referred to as ZnO/SOD.

Apparatus and Measurements. A CHI 660 electrochemical work station (CH Instruments) was employed in all electrochemical measurements. The geometric surface area of the working electrode employed in the analytical measurements was 0.02 cm^2. The reference electrode was a KCl-saturated Ag|AgCl electrode, while the auxiliary electrode was a platinum wire. An X-ray diffraction (XRD) pattern was obtained by a D/max2550VB3+/PC X-ray diffractormeter using Cu (40 kV, 100 mA). UV−vis absorption spectrum was recorded by an Agilent 8453 UV−vis−NIR spectrophotometer (Agilent Instruments). The $O_2^{\bullet-}$ solutions were prepared by the addition of aliquots of KO_2 stock solution (N_2-saturated). The concentration of $O_2^{\bullet-}$ was determined by recording the reduction of ferricytochrome *c* spectrophotometrically and using the extinction coefficient (21.1 mM^{-1} cm^{-1}) of ferrocytochrome *c* at 550 nm.[46]

In Vivo Experiments. Bean sprouts grown under environmental stress such as hyperoxia were selected as an in vivo model for $O_2^{\bullet-}$ determination in plants in the present work. Bean sprouts were prepared as follows: the seed of mung bean was washed with 70% ethanol and deionized water and then stocked in a 300-mL beaker with deionized water for one day to absorb enough water. After that, the seed was planted on the agar substrate. Bean sprout grown under hyperoxia (induced by excess $O_2^{\bullet-}$) was generated by exposing it to excess O_2 into the beaker (under saturated O_2 atmosphere) for at least 6 days and keeping it during all the experimental processes. For the controlled experiments, the bean sprout was grown under normal air atmosphere (21% O_2, 25 °C). In vivo experiments were carried out in a two-electrode electrochemical system as shown in Scheme 1, in which a ZnO/SOD microelectrode was employed as working electrode, with a Pt wire as counter electrode. A ZnO/SOD microelectrode was fabricated as follows: an ITO-coated glass plate was first cut into a spiny shape as shown in the inset of Scheme 1. Then, a ZnO nanodisk microelectrode was electrodeposited on a spiny-shaped ITO glass plate and was modified with Cu, Zn-SOD under the same experimental conditions as described above.

Scheme 1. Schematic Illustration of Setup for in Vivo Detection of $O_2^{\bullet-}$ in a Bean Sprout

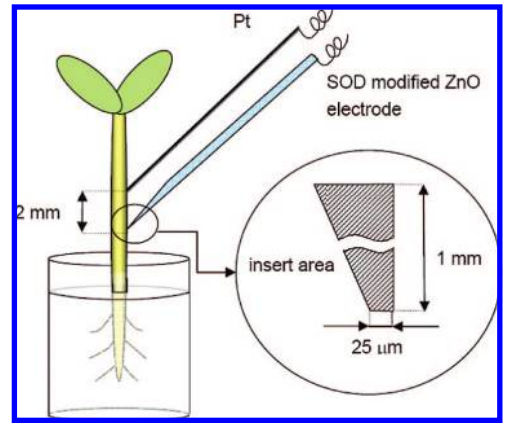

RESULTS AND DISCUSSION

Characterization of ZnO Nanodisks Film. A ZnO nanodisks film was fabricated by one-step electrodeposition as described in the Experimental Section and was characterized by scanning electron microscopy (SEM) as shown in Figure 1. The ZnO nanodisks are typically 50−80 nm in thickness and several micrometers in dimension, not free-standing. Many nanodisks are rather regular hexagons, and the contrast on a whole sheet is homogeneous. Moreover, many nanodisks have regular edges with an angle of 120°, which corresponds to the angles between the {01−10} planes of the wurtzite ZnO crystal structure.[47]

Figure 2 shows the optical absorbance spectrum of the nanostructured ZnO film. A sharp transition at ∼369 nm corresponding to 3.36 eV was observed. This corresponds to the bulk value of the band gap of ZnO.[47,48] The crystalline orientation of nanostructured ZnO film was investigated by recording the X-ray diffraction (XRD) pattern. The diffraction peaks of the ITO film and electrodeposited ZnO nanostructures are shown in Figure 3a and b, respectively. The pronounced peaks located at 31.8, 34.4, and 36.3° shown in Figure 3b, correspond to (100), (002), and (101) facets, indicating that the ZnO film has a polycrystalline hexagonal wurtzite structures.[47,48] The (222), (441), and (622) peaks of the ITO substrate are also observed as marked in Figure 3a.[49–51]

Direct Electrochemistry of SOD at the Nanostructured ZnO Film. From Figure 4, only the charge current was observed at the ZnO nanodisks surface (a), while a well-defined redox wave was obtained at the ZnO/SOD electrode (b) in 25 mM PBS (pH 7.2) containing no SOD. At the nanostructured ZnO disks surface,

(46) Fridovich, I. *J. Biol. Chem.* **1970**, *245*, 4053–4057.
(47) Cao, B.; Cai, W. J. *J. Phys. Chem. C.* In press.
(48) Zhang, H.; Cui, Y.; Men, Y.; Liu, X. *J. Lumin.* **2006**, *121*, 601–605.
(49) Tian, Y.; Liu, H.; Zhao, G.; Tatsuma, T. *J. Phys. Chem. B* **2006**, *110*, 23478–23481.
(50) Tian, Y.; Liu, H.; Deng, Z. *Chem. Mater.* **2006**, *18*, 5820–5822.
(51) Liu, H.; Tian, Y.; Deng, Z. *Langmuir* **2007**, *23*, 9487–9494.
(52) Fee, J. A.; DiCorleto, P. E. *Biochemistry* **1973**, *12*, 4893–4899.
(53) Clair, C. S. St.; Gray, H. B.; Valentine, J. S. *Inorg. Chem.* **1992**, *31*, 925–927.

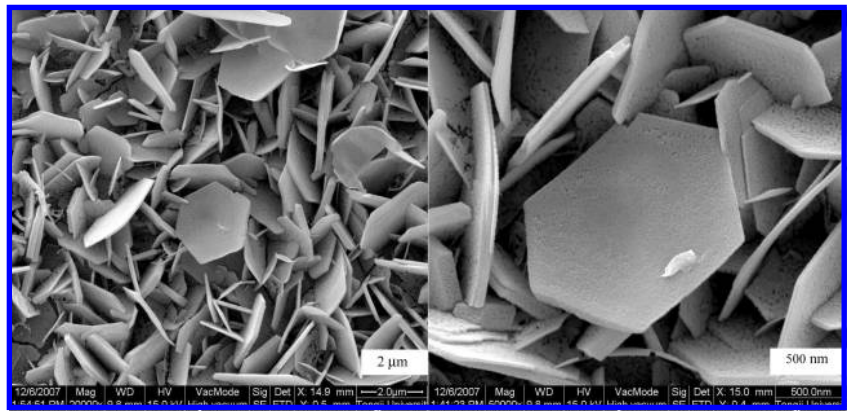

Figure 1. SEM images of electrodeposited ZnO nanodisks film.

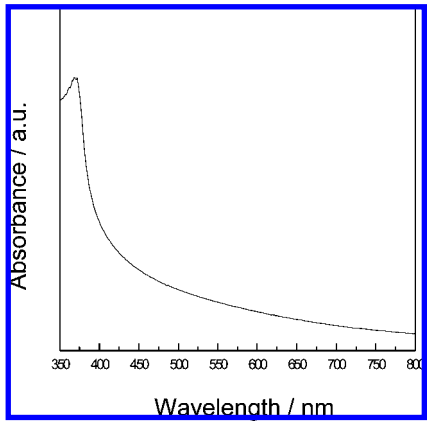

Figure 2. UV−vis absorption spectrum of the ZnO nanodisks film.

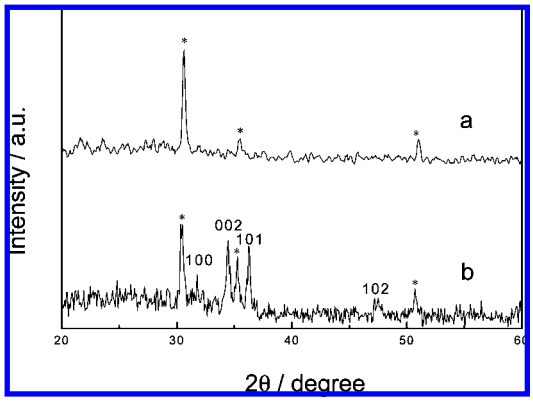

Figure 3. X-ray diffraction patterns of ITO (a) and the ZnO nanodisks film (b).

a pair of redox peaks of SOD was observed with a peak width at half-peak height ($\Delta E_{p,1/2}$) of 82 ± 3 mV (n = 4). The formal potential ($E^{0'} = (E_{p,a} + E_{p,c})/2$) of SOD confined on ZnO film was estimated to be 108 ± 6 mV (n = 4) versus Ag|AgCl. The value is within a range from 40 to 212 mV versus Ag|AgCl reported previously for the direct electron transfer of SODs in the neutral phosphate buffer solution.[25,28,29,54] The diversity in these values is probably due to the differences in enzyme preparation and electron-transfer surfaces.

(54) Beissenhirtz, M. K.; Scheller, F. W.; Viezzoli, M. S.; Lisdat, F. *Anal. Chem.* **2006**, *78*, 928–935.

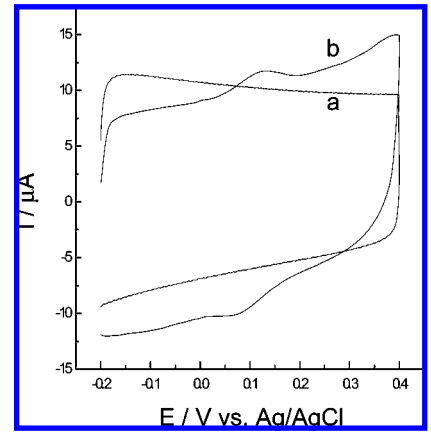

Figure 4. CVs obtained at (a) bare ZnO nanodisks film and (b) ZnO/SOD film in 25 mM PBS (pH 7.2); Potential scan rate, 500 mV s^{-1}.

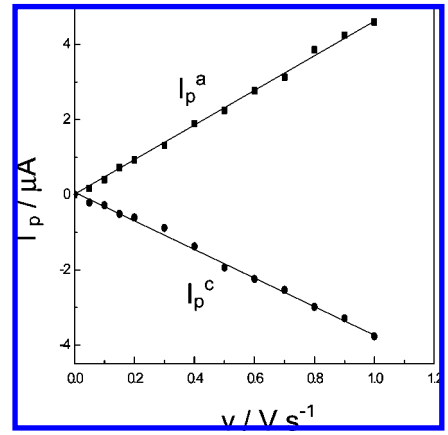

Figure 5. Relationship between anodic and cathodic peak currents of ZnO/SOD film and scan rate.

CVs of the ZnO/SOD electrode at various scan rates are also obtained in fresh buffer solution containing no SOD. It was found that both the anodic and cathodic peak currents (I_p^a and I_p^c) vary linearly with potential scan rate (v) in the range of 50−1000 mV s^{-1} (Figure 5). In addition, the CVs remained essentially unchanged on consecutive potential scanning up to 1000 cycles at a sweep rate of 20 mV s^{-1}, indicating that SOD was stably immobilized on the nanostructured ZnO disks film. According to Laviron's procedure,[55] the relevant kinetic parameters of the

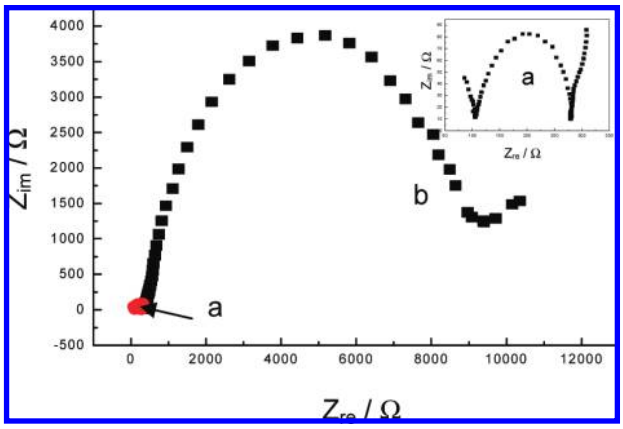

Figure 6. Nyquist plots obtained at (a) bare ZnO nanodisks film (enlarged in the inset) and (b) ZnO/SOD electrode in 0.1 M KCl solution containing 1 mM $[Fe(CN)_6]^{3-/4-}$. EIS conditions: potential, 0.25 V; alternative voltage, 5 mV; frequency range, 0.1−10^5 Hz.

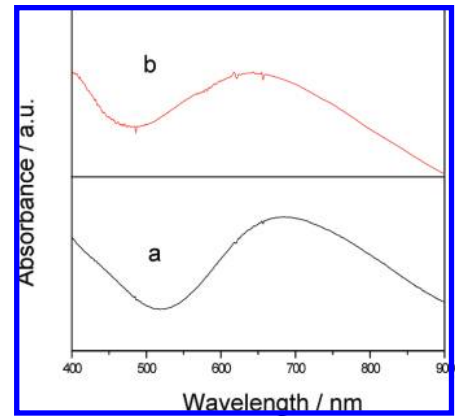

Figure 7. UV−vis absorption spectra of (a) 0.2 mM SOD solution and (b) SOD confined on the ZnO nanodisks film.

electrode reaction, i.e., the rate constant of the electrochemical process (k_s) and cathodic transfer coefficients (α_c), were estimated: $k_s = 17 \pm 2\ s^{-1}$, $\alpha_c = 0.52 \pm 0.02$ ($n = 4$) at the nanostructured ZnO surface. It reveals that the direct electron transfer of SOD is strikingly enhanced at the nanostructured ZnO surface. ZnO/SOD nanocomposites show reversible electrochemistry with formal potential of 108 ± 6 mV versus Ag|AgCl and k_s value of 17 ± 2 s^{-1}. The electron-transfer rate of SOD on the nanostructured ZnO surface is higher than those obtained at the promoter-modified gold surfaces,[25,28,29] suggesting the loss of promoters may shorten the distance between the copper moiety of SOD and the ZnO nanostructures and, in turn, favor the electron transfer of SOD. In addition, the calculated electron-transfer rate of SOD on the nanostructured ZnO film is slightly higher, compared with those obtained in sol−gel films and at CNT surfaces, implying that the ZnO nanodisks may be more favorable for the electron transfer of SOD than thin silica−PVA sol−gel film or CNT.[56,57]

The adsorbed behavior of SOD was confirmed by EIS. Figure 6 shows Nyquist plots obtained at bare ZnO nanodisks film and ZnO/SOD electrode in 0.1 M KCl solution containing 0.1 M $[Fe(CN)_6]^{3-/4-}$. The charge-transfer resistance (R_{ct}) of the $Fe(CN)_6^{3-/4-}$ redox couple is ~174 Ω at ZnO nanodisks film (Figure 6a), but it increases by a near 10^3-fold, to 9.7 KΩ after SOD was immobilized on ZnO nanodisks as shown in Figure 7b. These data suggested that SOD adsorbed onto the nanostructured ZnO surface might inhibit the electrochemical communication between the electron-transfer indicator—$Fe(CN)_6^{3-/4-}$— and the nanostructured ZnO electrode, resulting in the great increase of R_{ct} of the $Fe(CN)_6^{3-/4-}$ redox couple.

Spectroscopic Characterization of SOD Adsorbed on the Nanostructured ZnO Surface. Direct electron transfer of SOD was greatly facilitated at the nanostructured ZnO surface, and experimental results demonstrated that SOD was stably confined on the ZnO nanodisks film. Therefore, it is desirable to clarify whether SOD retains its inherent activity for dismutation of $O_2^{\bullet-}$ after immobilization on the ZnO nanostructures, which enables the direct electron transfer of SOD itself. The activity of SOD toward $O_2^{\bullet-}$ adsorbed on the ZnO nanodisks film was characterized by UV−vis absorption spectroscopy since the activity of SOD is closely related to the molecule structure of the Cu^{2+} site.[58] Figure 7 depicts UV−vis absorption spectra of 0.2 mM SOD in solution (a) and SOD confined on the optical transparent ZnO nanodisks surface (b). The two spectra are similar and have an absorption peak located at the range of 650−750 nm, corresponding to the characteristic of Cu^{2+} site of SOD.[58] This observation revealed that SOD almost processed its intrinsic activity for dismutation of $O_2^{\bullet-}$ after being adsorbed on the nanostructured ZnO film, because the peak will be diminished if the protein is denaturated.[38,59] To confirm this point, the UV−vis absorption spectrum of mixed SOD and CN^- solution was measured (data not shown) because SOD is reported to be inhibited and denaturated by singly charged anions such as CN^-, N_3^-, and F^-.[60,61] As a result, no absorption peak was observed of the SOD solution that had been denaturated with 50 mM CN^-.

Selectivity, Linearity, Stability, and Reproducibility. As demonstrated above, SOD processes its enzymatic activity after being adsorbed on the nanostructured ZnO surface, which also facilitates the electron transfer of SOD itself. This result formed a strong basis for the development of a third-generation biosensor for $O_2^{\bullet-}$ because SOD catalyzes the dismutation of $O_2^{\bullet-}$ to O_2 and H_2O_2 via a cyclic oxidation−reduction electron transfer. The interaction of $O_2^{\bullet-}$ and SOD was studied using cyclic voltammetry. Figure 8 compares the CVs obtained at the ZnO/SOD-based electrode in the absence (curve a) and in the presence (curve b) of $O_2^{\bullet-}$. Both currents in the oxidation and reduction regions increased in the presence of $O_2^{\bullet-}$. The assignment of the increased anodic and cathodic currents to the oxidation and reduction of $O_2^{\bullet-}$ was confirmed by adding SOD, a selective scavenger of $O_2^{\bullet-}$, into the solution containing $O_2^{\bullet-}$. As expected, both peaks shrank quickly and almost returned to the curve a when SOD solution was added into the measured solution because $O_2^{\bullet-}$ was removed by SOD from solution.In addition, such a redox response was not

(55) Laviron, E. *J. Electroanal. Chem.* **1979**, *101*, 19–28.
(56) Bi, Y.; Huang, Z.; Zhao, Y. *Biosens. Bioelectron.* **2006**, *21*, 1350–1354.
(57) Di, J.; Bi, S.; Zhang, M. *Biosens. Bioelectron.* **2004**, *19*, 1479–1486.
(58) Vedejs, E.; Martinez, G. R. *J. Am. Chem. Soc.* **1979**, *101*, 6454–6456.
(59) Nassar, A. F.; Willis, W. S.; J.F.Rusling, J. F. *Anal. Chem.* **1995**, *67*, 2386–2392.
(60) Rotilio, G.; Morpurgo, L.; Giovagnoli, C.; Calabrese, L.; Mondovi, B. *Biochemistry* **1972**, *11*, 2187–2192.
(61) Bertini, I.; Luchinat, C.; Scozzafava, A. *J. Am. Chem. Soc.* **1980**, *102*, 7349–7353.

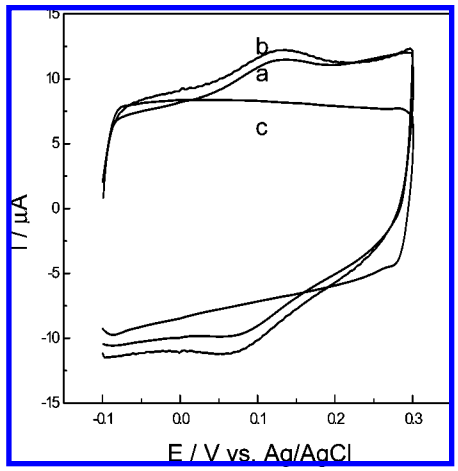

Figure 8. CVs obtained at ZnO/SOD (a, b) and bare ZnO nanodisks (c) electrodes in the absence (a) and presence (b, c) of 30 μM $O_2^{\bullet-}$ in 25 mM PBS (pH 7.2). Potential scan rate, 500 mV s^{-1}.

observed at the bare ZnO nanodisks electrode in the presence of $O_2^{\bullet-}$ (curve c). Therefore, we can consider that the observed increase in the anodic and cathodic current responses of the ZnO/SOD electrode in the presence of $O_2^{\bullet-}$ can be ascribed to the oxidation and reduction of $O_2^{\bullet-}$, respectively, which are effectively mediated by the SOD confined on the electrode. These data also suggest that SOD adsorbed on the ZnO nanodisks film processes its enzymatic activity toward $O_2^{\bullet-}$ dismutation.

The following reaction mechanism could explain the enhanced oxidation current observed in Figure 8.

$$\text{SOD(Cu(I))} - e \longrightarrow \text{SOD(Cu(II))} \quad (1)$$

$$\text{SOD(Cu(II))} + O_2^{\bullet-} \longrightarrow \text{SOD(Cu(I))} + O_2 \quad (2)$$

Similarly, the reduction current is enhanced in the cathodic scan according to the following scheme:

$$\text{SOD(Cu(II))} + e \longrightarrow \text{SOD(Cu(I))} \quad (3)$$

$$\text{SOD(Cu(I))} + O_2^{\bullet-} \xrightarrow{H^+} \text{SOD(Cu(II))} + H_2O_2 \quad (4)$$

Amperometric responses of ZnO/SOD, to successive concentration changes of $O_2^{\bullet-}$ were conducted at the applied potential of +300 and 0 mV, and the corresponding current−time responses are shown in Figure 9A and B, respectively. Well-defined steady-state current responses were obtained at both +300 and 0 mV, and the currents increased stepwise with successive additions of $O_2^{\bullet-}$. The optimized surface area of working electrode was determined to be 0.02 cm^2, for obtaining the steady-state current responses. The anodic and cathodic calibration plots are shown in Figure 10A and B, respectively. The analytical characteristic of the present $O_2^{\bullet-}$ biosensors at the optimized conditions were summarized in Table 1. From Table 1, we can see that ZnO/SOD electrode shows excellent analytical performance, for instance, wider linear detection range, lower detection limit, and shorter response time, compared to the other $O_2^{\bullet-}$ biosensors based on the direct electrochemistry of Cu, Zn-SOD in sol−gel film and at

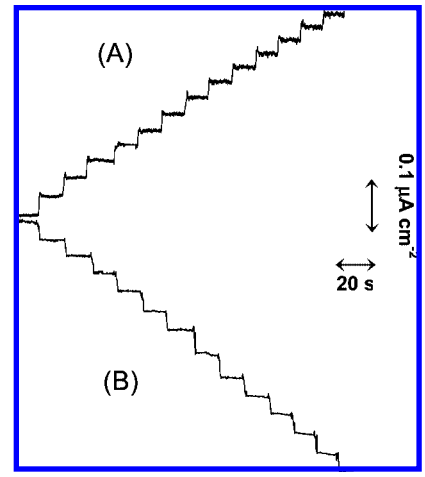

Figure 9. Typical amperometric responses of the ZnO/SOD to successive additions of 4 μL of KO_2 (10 μM) at applied potentials of (A) +300 and (B) 0 mV in 2 mL of PBS (25 mM, pH 7.2). The same electrode was employed in both anodic and cathodic measurements.

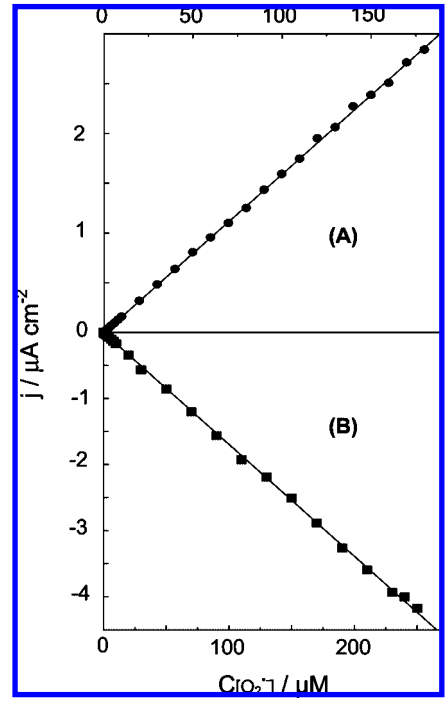

Figure 10. Calibration plots of anodic (A) and cathodic (B) steady-state currents against concentration of $O_2^{\bullet-}$. Data were obtained from Figure 9.

Table 1. Analytical Properties of the $O_2^{\bullet-}$ Biosensors Based on ZnO/SOD Nanocomposites

	ZnO/SOD	
applied potential (mV)	300	0
sensitivity (nA cm^{-2}/μM)	15.9 ± 0.6	17.1 ± 0.4
response time (s)	4	4
linear range (μM)	0.24−180	0.12−250
detection limit (μM)	0.2	0.1

the CNT surface, without any mediators or promoters.[56,57] In particular, the dynamic linear range for detection of $O_2^{\bullet-}$ from 120 nM to 0.25 mM at the applied potential of 0 mV,

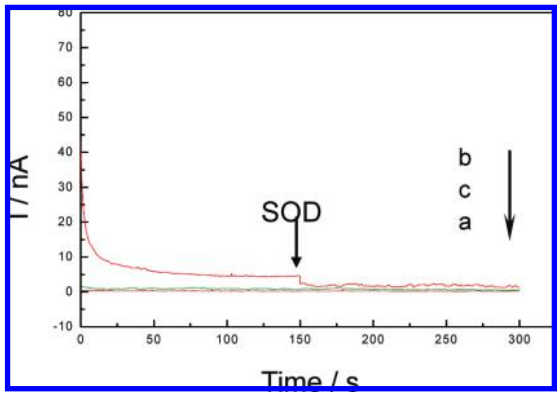

Figure 11. Amperometric responses of ZnO/SOD microelectrode (a, b) and ZnO microelectrode (c) recorded at the applied potential of −0.5 V vs Pt (−0.03 V vs Ag|AgCl) in a bean sprout grown under air atmosphere (a) and under hyperoxia (b, c) for 6 days.

is much wider than that obtained in our previous $O_2^{\bullet-}$ biosensors,[26,28,30] and fulfills the requirement of in vivo tracking of $O_2^{\bullet-}$ concentration, as described above.

As is well-known, the coexisting biological compounds may result in difficulties for in vivo electrochemical determinations. The present bidirectional catalytic activity of the SOD toward $O_2^{\bullet-}$ dismutation essentially allowed us to detect $O_2^{\bullet-}$ by polarizing the electrode either anodically or cathodically. Such a distinct feature efficiently avoids the potential interferences. The interferences from uric acid (UA), ascorbic acid (AA), 3,4-dihydroxyphenylacetic acid (DOPAC), and H_2O_2 were investigated at +300 and 0 mV. At +300 mV, 3.7 and 5.5% current responses were obtained for 15 μM AA and 20 μM UA relative to 4 μM $O_2^{\bullet-}$ with the ZnO/SOD electrode, respectively. However, such interferences were well-suppressed when the electrodes were polarized at 0 mV. In addition, the interferences of H_2O_2, O_2, and DOPAC were negligible (<1%) at both +300 and 0 mV.

For the stability test, both the anodic and cathodic responses for $O_2^{\bullet-}$ were recorded three times daily and the current responses were found to be constant for at least one month, which holds relatively longer stability than that obtained at the CNT-SOD $O_2^{\bullet-}$ biosensor[56] and our previous SODs-based $O_2^{\bullet-}$ biosensors[26,28,30] at gold electrodes. In addition, we have found that the deviation of the current responses of over five sensors prepared with the same method did not exceed 4.8%.

Accordingly, superior to the previous $O_2^{\bullet-}$ biosensors,[26,28,30] SOD adsorbed on the ZnO nanodisks film is capable of sensing $O_2^{\bullet-}$ cathodically at a very positive potential, 0 mV (vs Ag|AgCl), where the common interfering species such as H_2O_2, UA, AA, and DOPAC were effectively avoided. Besides this, it shows remarkable analytical properties such as wide dynamical linear range, long stability, and good reproducibility. These excellent analytical performances, together with notable characteristics of the ZnO nanodisks film, such as biocompatibility, ease of preparation, and ability to miniaturize, eventually gave us a strong basis for in vivo determination of $O_2^{\bullet-}$.

In Vivo Detection of $O_2^{\bullet-}$ in the Bean Sprout. Figure 11 depicts amperometric responses of the ZnO/SOD microelectrode recorded at the applied potential of −0.5 V versus Pt (−0.03 V vs Ag|AgCl) in bean sprouts grown under air atmosphere (a), and under hyperoxia (b) for 6 days. We can see that the cathodic current observed in a bean sprout grown under hyperoxia is greater than that generated in the same bean sprout under air atmosphere. Interestingly, after injection of 10 μL of 0.2 M SOD solution, a selective scavenger of $O_2^{\bullet-}$, into the bean sprout at the vicinity of the working electrode, the current shown in curve b decreased rapidly and went down to the almost background value of curve a in 5 s. For the comparison, current−time response of bare ZnO nanodisks film was also recorded in the same plant grown under hyperoxia and is given as curve c, which is at almost the same level as curve a. It revealed that the direct reduction of $O_2^{\bullet-}$ at a bare ZnO film could be negligible, compared with that obtained at a ZnO/SOD film. So, we can conclude that the generated increase of cathodic current at a ZnO/SOD microelectrode in the bean sprout grown under hyperoxia is ascribed to the enzymatic reduction of $O_2^{\bullet-}$, which is effectively mediated by the SOD confined on the electrode. Similarly, the increase of anodic current was also obtained at ZnO/SOD microelectrode in a bean grout grown under hyperoxia, at the applied potential of −0.05 V versus Pt (+0.42 V vs Ag|AgCl, data not shown).

For the durability test, amperometric responses of ZnO/SOD microelectrode obtained in a bean sprout grown under air atmosphere, and under hyperoxia, from the 6th day to the 12th day were recorded at the applied potential of −0.5 V versus Pt. We found that the deviation of the current responses of continuous measurements for 7 days did not exceed 10%. This observation substantially demonstrates the present developed third-generation $O_2^{\bullet-}$ biosensor with nanostructured ZnO microelectrode provides an in vivo model for reliable and durable determination of $O_2^{\bullet-}$ in plants and could be potentially useful for physiological and pathological investigations Table 1.

CONCLUSIONS

Direct electron transfer of Cu, Zn-SOD was achieved at the ZnO nanodisks film, which was successfully fabricated by a one-step, low-cost, no-template electrodeposited method, with high heterogeneous electron-transfer rate constant. The nanostructured ZnO film stably immobilized SOD molecules, and spectroscopic data suggested that SOD held its inherent enzymatic activity toward $O_2^{\bullet-}$ dismutation after being confined on the ZnO film. The remarkably facilitated electron transfer of SOD, combined with the intrinsic bidirectional catalytic activity of the SOD essentially allowed us to develop a third-generation $O_2^{\bullet-}$ biosensor. Besides high selectivity, the present $O_2^{\bullet-}$ biosensor showed excellent analytical performance, such as wider linear range, longer stability, and better reproducibility, compared to the previous $O_2^{\bullet-}$ biosensors. The remarkable analytical characteristics, together with the intrinsic properties of ZnO nanostructures, such as biocompatibility, ease of preparation, and ability to miniaturize, sufficiently offered an electrochemical approach to in vivo detection of $O_2^{\bullet-}$ in bean sprout. This investigation not only opened a way to realize direct electron transfer of proteins or enzymes on nanostructured semiconductor film and on the basis of this platform to construct third-generation biosensors, but also provided an in

vivo model for $O_2^{\bullet-}$ determination in a biological system, in which more understanding could be gained of the role that $O_2^{\bullet-}$ and ROS play in pathology and physiology.

ACKNOWLEDGMENT

This work was financially supported by the National Natural Science Foundation of China (20643002), Program for New Century Excellent Talents in University (NCET-06-0380), and the Scientific Research Foundation for the Returned Overseas Chinese Scholars from State Education Ministry, China, and Shanghai Pujiang Program (06PJ14090). Tongji University is also greatly acknowledged.

Received for review January 29, 2008. Accepted May 19, 2008.

AC800213X